Hindawi Publishing Corporation
Journal of Structures
Volume 2013, Article ID 942302, 9 pages
http://dx.doi.org/10.1155/2013/942302

Research Article

Structural Preferences and Vibrational Analysis of 2-Hydroxy-2-methyl-1-phenylpropan-1-one: A Computational and Infrared Spectroscopic Research

O. Belaidi,[1] T. Bouchaour,[1] and U. Maschke[2]

[1] *Laboratoire de Recherche sur les Macromolécules, Faculté des Sciences, Université Abou Bekr Belkaid, BP119, 13000 Tlemcen, Algeria*
[2] *Unité Matériaux et Transformations (UMET), UMR CNRS N° 8207, Université Lille 1-Sciences et Technologies, 59655 Villeneuve d'Ascq Cedex, France*

Correspondence should be addressed to O. Belaidi; othmanblaidi@gmail.com

Received 13 February 2013; Revised 6 May 2013; Accepted 11 May 2013

Academic Editor: Elsa Caetano

The Fourier transform infrared (FTIR) spectrum of 2-hydroxy-2-methyl-1-phenylpropan-1-one has been measured in the region 4000–700 cm^{-1}. The most stable conformation of title molecule was found after a careful potential energy surfaces study. The molecular geometry, vibrational frequencies, and infrared intensities have been calculated by using ab initio HF and density functional theory calculation B3LYP with 6-311+G** basis set. Scaled frequencies and potential energy distribution were calculated for band assignment. We found an excellent agreement between the experimental and the simulated spectra. Energy gap between HOMO and LUMO explains the eventual charge transfer interactions taking place within the molecule.

1. Introduction

The radiation curing industry is one of the most rapidly developing fields in the entire coating industry. The low toxicity, cheapness, speed, control, and ease of formulation and operation are some of the main advantages of this growing technology. UV and/or visible light radiation is used to induce photochemical polymerization or cross-linking of a monomer, oligomer, or prepolymer formulation containing a certain type of unsaturation, such as an acrylic group, and an appropriate initiator [1, 2]. Among the large group of known photoinitiator structures, hydroxyalkylphenones, such as 2-hydroxy-2-methyl-1-phenylpropan-1-one (Figure 1), have gained much interest due to their high reactivity and universal applicability [3, 4].

Despite the high practical value of title molecule, its physicochemical properties have been relatively little looked into [8–12].

To our best knowledge no structural data and detailed interpretation of the vibrational spectra of the title molecule are presented in the literature. This prompted us to look into the vibrational spectroscopy of the title molecule more carefully.

2. Experimental

2-Hydroxy-2-methyl-1-phenylpropan-1-one (purity 97%) was purchased from Sigma-Aldrich and used as such without further purification. The infrared spectra of liquid films placed between KBr pellets were recorded within 4000–700 cm^{-1} range with a Perkin Elmer FTIR System-2000 model.

3. Computational

Potential energy curves were obtained by calculating the variation of total energy of title molecule with dihedral angles. For this purpose the calculations were performed with B3LYP functional and 6-311+G** basis set. The dihedral angles were varied from 0° to 360° with an interval of 10°.

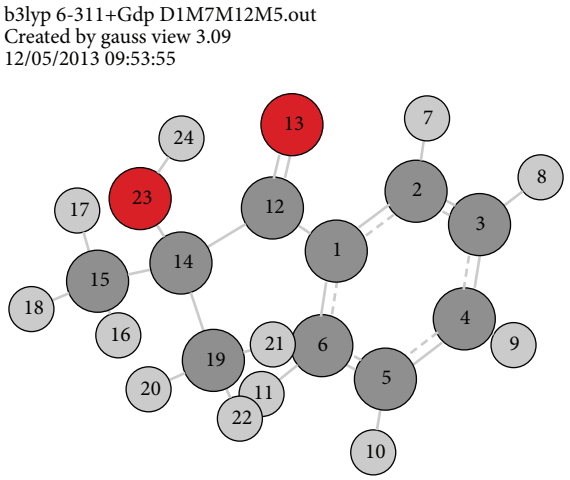

Figure 1: The optimized geometrical structure with atoms numbering of 2-hydroxy-2-methyl-1-phenylpropan-1-one.

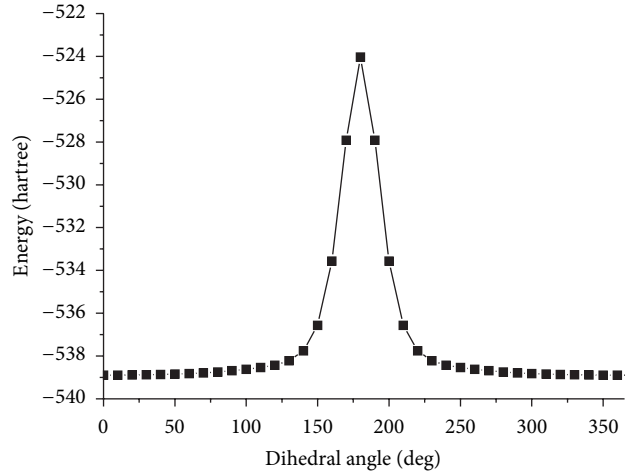

Figure 2: Potential energy curves of 2-hydroxy-2-methyl-1-phenylpropan-1-one for rotation about C1C12(–■–).

All DFT calculations were performed using Becke's 3 parameter (local, nonlocal, Hartree-Fock) hybrid exchange functionals with Lee-Yang-parr correlational functionals (B3LYP) [13, 14].

The harmonic vibrational frequencies of the stable conformation were calculated at the same level of theories used for the calculated optimized geometry. Two levels of theory were used for vibrational analysis B3LYP/6-311+G** and HF/6-311+G**; the calculated frequencies were scaled down by the wavenumber linear scaling (WLS) procedure of Yoshida et al. [15, 16] using the following equation, for DFT:

$$\frac{\nu_{\text{obs}}}{\nu_{\text{calc}}} = 1.0087 - 0.0000163\nu_{\text{calc}} \quad (1)$$

and the scaling factor proposed by Baker et al. [17] for HF. The scaling procedures are used due to the fact that the anharmonic effects are neglected when calculating wavenumbers at HF and DFT theories, which make the calculated value higher than the experimental one. All the calculations were carried out with the Gaussian 03 program [18]. The vibrational assignments of normal modes were provided on the basis of PED calculation using the program GAR2PED [19].

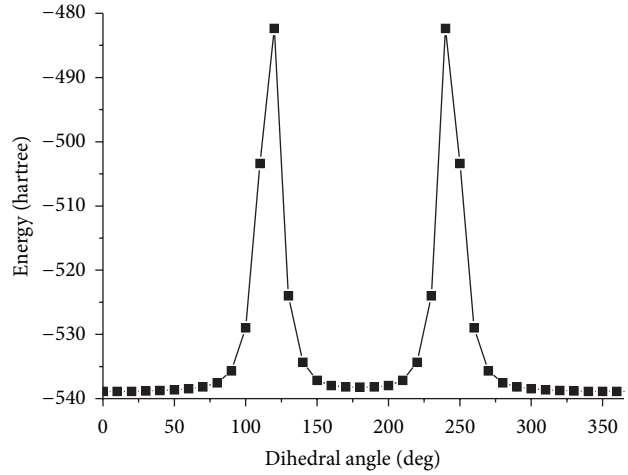

Figure 3: Potential energy curves of 2-hydroxy-2-methyl-1-phenylpropan-1-one for rotation about C12C14(–■–).

4. Conformational Analysis

Due to the flexibility of 2-hydroxy-2-methyl-1-phenylpropan-1-one and possible rotational isomerism, we examined the variation of energy with respect to $C_6C_1C_{12}C_{14}$, $C_1C_{12}C_{14}C_{23}$, and $C_{12}C_{14}C_{23}O_{24}$ dihedral angles. From Figure 2 we see that the energy is increasing when increasing dihedral angle to a maximum in energy of $-3.25\,10^5$ kcal/mol at 180°. There is only one minimum at 0° with an energy of $-3.38\,10^5$ kcal/mol.

It is well seen from Figures 3 and 4 that the molecule takes two minima at 0° and 180°. In Figure 3 the difference in energy between the two minima is 419.7 kcal/mol, and it is 8.785 kcal/mol in Figure 4.

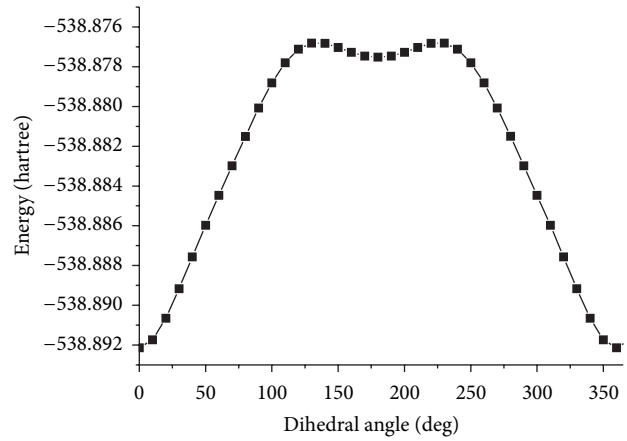

Figure 4: Potential energy curves of 2-hydroxy-2-methyl-1-phenylpropan-1-one for rotation about C14O23(–■–).

The potential energy surfaces revealed the existence of tree conformers. The energy of the most stable conformation is $-3.38\,10^5$ kcal/mol.

5. Geometry Optimizations

The most stable structure is recognized as true minima due to the lack of imaginary harmonic frequencies. The geometry parameters are represented in Table 1. To the best of our knowledge, exact experimental data of the geometrical parameters of the 2-hydroxy-2-methyl-1-phenylpropan-1-one are not available in the literature. Therefore our optimized structural parameters are compared with the XRD data of closely related molecules benzoic acid and butyric acid [5, 6]. The theoretical results are almost comparable with the experimental XRD values. The carbon-oxygen $C_{14}O_{23}$ = 1.421 and carbon-carbon $C_{12}C_{14}$ = 1.554, $C_{14}C_{15}$ = 1.540, and C14C19=1.540 bond lengths are in agreement with the XRD values [7] 1.38, 1.55, 1.54, and 1.54, respectively. In the phenyl ring, the bond lengths and the bond angles are in good agreement with the experimental one [7]. Thus the ring is slightly distorted and smaller than 120° at the point of substitution.

In Table 1, a small difference between the two levels of theory HF and DFT should be noticed for the calculated coordinates. The bond lengths are less estimated by HF with a maximum difference of 0.01A°. However, this difference is about 0.02A° for C14O23 bond. The B3LYP calculations lead to a planar structure of the phenyl ring, ketone and hydroxyl groups. Otherwise, these groups lie in a near planar form according to the HF optimization. This could be seen directly from dihedral angles ($C_6C_1C_{12}O_{13}$, $C_6C_1C_{12}C_{14}$, $C_1C_{12}C_{14}C_{15}$, $C_1C_{12}C_{14}C_{19}$, $C_1C_{12}C_{14}O_{23}$, and $C_{12}C_{14}O_{23}H_{24}$) deviating about 10° from those obtained by B3LYP level of theory.

The zero point corrected energy for the most stable structure of the title molecule is $-337.911\,10^3$ kcal/mol at B3LYP/6-311+G** and $-335.786\,10^3$ kcal/mol at HF/6-311+G**. The energy calculated by DFT is lower showing more stability than that calculated at HF method.

6. Vibrational Analysis

The title compound contains 24 atoms leading to 66 normal vibrational modes. We compared the experimental IR spectrum with the computed IR spectrum, and we checked whether we can recognize all the different bands. Table 2 represents the calculated and scaled fundamental wavenumbers, intensities of vibrational peaks, and PED calculations along the internal coordinates obtained by B3LYP/6-311+G** level of theory. The corresponding experimental wavenumbers together with assignments and potential energy distribution are also reported in this table. Assignments have been made on the basis of PED, and they are given as per the internal coordinate system recommended by Pulay et al. using DFT [20]. The experimental and theoretical spectra are shown in Figure 5.

Table 1: Optimized geometry of 2-hydroxy-2-methyl-1-phenyl-propan-1-one calculated at HF and B3LYP using 6-311+G** basis set.

Internal coordinates	Level of theory		
	RHF/6-311+G**	DFT/6-311+G**	X-ray[a]
Bond lengths (Å)			
C_1C_2	1.395	1.405	1.39
C_2C_3	1.381	1.388	1.41
C_3C_4	1.386	1.395	1.37
C_4C_5	1.383	1.392	1.36
C_5C_6	1.385	1.392	1.42
C_6C_1	1.390	1.402	1.39
$CH_{(ring)\ average}$	1.073	1.082	
C_1C_{12}	1.506	1.499	1.48
$C_{12}O_{13}$	1.194	1.221	1.24
$C_{12}C_{14}$	1.547	1.554	1.55[b]
$C_{14}C_{15}$	1.535	1.540	1.54[b]
$C_{15}H_{16}$	1.082	1.090	
$C_{15}H_{17}$	1.085	1.092	
$C_{15}H_{18}$	1.084	1.092	
$C_{14}C_{19}$	1.531	1.540	1.54[b]
$C_{19}H_{20}$	1.084	1.092	
$C_{19}H_{21}$	1.085	1.092	
$C_{19}H_{22}$	1.081	1.090	
$C_{14}O_{23}$	1.399	1.421	1.38[b]
$O_{23}H_{24}$	0.944	0.971	0.95
Bond angles (°)			
$C_1C_2C_3$	120.8	120.9	120
$C_2C_3C_4$	119.9	120.0	122
$C_3C_4C_5$	119.7	119.7	118
$C_4C_5C_6$	120.1	120.2	123
$C_5C_6C_1$	120.6	120.6	118
$C_6C_1C_2$	118.5	118.4	119
$CCH_{ring\ average}$	119.4	119.3	
$C_6C_1C_{12}$	125.1	124.8	
$C_1C_{12}O_{13}$	118.7	119.2	118
$C_1C_{12}C_{14}$	124.0	123.9	
$C_{12}C_{14}C_{15}$	110.5	111.3	
$C_{14}C_{15}H_{16}$	113.6	113.4	
$C_{14}C_{15}H_{17}$	110.0	110.1	
$C_{14}C_{15}H_{18}$	108.0	107.9	
$C_{12}C_{14}C_{19}$	112.3	111.3	
$C_{14}C_{19}H_{20}$	107.9	107.9	
$C_{14}C_{19}H_{21}$	110.2	110.1	
$C_{14}C_{19}H_{22}$	113.4	113.4	
$C_{12}C_{14}O_{23}$	107.4	107.2	
$C_{14}O_{23}H_{24}$	109.0	106.2	111
Dihedral angles (°)			
$C_1C_2C_3C_4$	0.4	0.0	
$C_2C_3C_4C_5$	−0.1	0.0	
$C_3C_4C_5C_6$	−0.2	0.0	

Table 1: Continued.

Internal coordinates	Level of theory		
	RHF/6-311+G**	DFT/6-311+G**	X-ray[a]
$C_6C_4C_2H_7$	179.7	180.0	
$C_1C_2C_3H_8$	−179.6	180.0	
$C_2C_3C_4H_9$	179.8	180.0	
$C_3C_4C_5H_{10}$	179.7	180.0	
$C_4C_5C_6H_{11}$	179.9	180.0	
$C_5C_6C_1C_{12}$	179.2	−179.9	
$C_6C_1C_{12}O_{13}$	−169.4	179.9	
$C_6C_1C_{12}C_{14}$	10.7	0.0	
$C_1C_{12}C_{14}C_{15}$	−71.3	−63.2	
$C_{12}C_{14}C_{15}H_{16}$	67.1	68.2	
$C_{12}C_{14}C_{15}H_{17}$	−54.6	−53.7	
$C_{12}C_{14}C_{15}H_{18}$	−172.2	−171.3	
$C_1C_{12}C_{14}C_{19}$	55.4	63.2	
$C_{12}C_{14}C_{19}H_{20}$	169.6	171.3	
$C_{12}C_{14}C_{19}H_{21}$	52.1	53.7	
$C_{12}C_{14}C_{19}H_{22}$	−69.9	−68.2	
$C_1C_{12}C_{14}O_{23}$	171.8	−179.9	
$C_{12}C_{14}O_{23}H_{24}$	11.2	0.0	

[a]XRD data of closely related molecules benzoic acid and butyric acid [5, 6].
[b]XRD data of 4-butyl-1-(4-hydroxyphenyl)-2-phenyl-3,5-pyrazolidinedione [7].

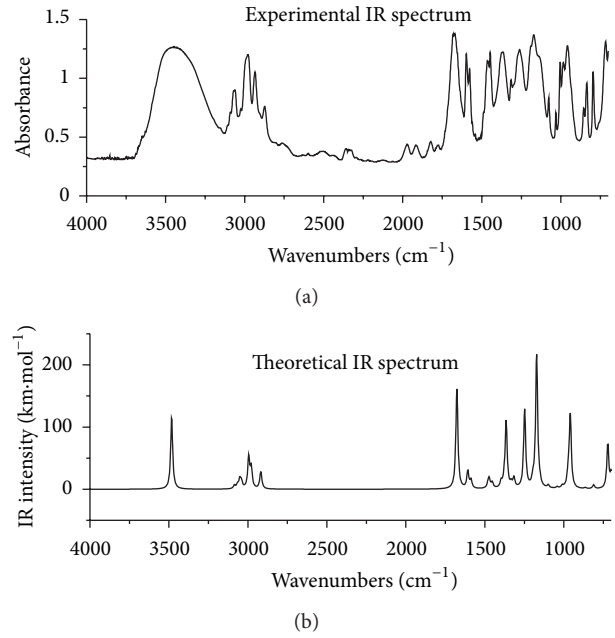

Figure 5: Experimental and theoretical infrared spectra of 2-hydroxy-2-methyl-1-phenylpropan-1-one.

6.1. Phenyl Ring Vibrations. The substituted-like molecule gives rise to CH stretching, CH in-plane and out-of-plane bending vibrations. The heteroaromatic structure shows the presence of CH stretching vibration in the region 3100–3000 cm^{-1} which is the characteristic region for the ready identification of CH stretching vibration [15, 21]. In this region the bands are not affected appreciably by the nature of the substituent. The aromatic CH stretching frequencies rise from the modes observed at 3062, 3047, 3060, and 3080 cm^{-1} of benzene and its derivatives [22].

In this work, the CH stretching vibrations are observed at 3025, 3060, 3070, 3090, and 3108 cm^{-1} in the FTIR. The calculated values of these modes for the title molecule have been found to be 3031, 3041, 3051, 3066, and 3085 cm^{-1} at the B3LYP/6-311+G** level of theory. The calculated PEDs for these normal modes are greater than 85% (see Table 2).

The CH-in plane bending vibrations usually occur in the region 1430–990 cm^{-1} and are very useful for characterization purposes. The band due to CH-in plane ring vibrations interacting somewhat with CC stretching vibration is observed as a number of medium-to-weak sharp bands in the region of 1300–1000 cm^{-1} [23, 24]. In this study, the FTIR peaks at 1077, 1170, 1192, and 1315 cm^{-1} are assigned to CH in-plane bending vibrations as reported in Table 2. The strong peak below 900 cm^{-1} indicates clearly the aromatic aspect of the molecule. Substitution patterns on the ring can be judged from the CH out-of-plane bending in the region 900–650 cm^{-1}, and these bands are highly informative [25]. The CH out-of-plane bending vibrations are strongly coupled vibrations in the region 900–667 cm^{-1} [26]. In the present study, the calculated frequencies at 994, 950, 857, 721, and 697 cm^{-1} may be assigned to the experimental bands at 934, 836, and 716 cm^{-1}. The calculated PEDs show that these bands are not pure CH out-of-plane bending vibrations.

The ring carbon-carbon stretching vibration occurs in the region 1625–1430 cm^{-1}. In general, the bands are of variable intensity and are observed at 1625–1590, 1590–1575, 1540–1470, 1460–1430, and 1380–1280 cm^{-1} from the frequency ranges given by Varsanyi [27] for the five bands in the region. In this work, the frequencies observed in the FTIR spectrum at 1598, 1578, 1489, and 1447 cm^{-1} are well reproduced by the theoretical frequencies at 1607, 1587, 1497, and 1452 cm^{-1}. The calculated PEDs show that these modes are not pure CC stretching vibrations. The normal mode no. 31 is attributed to the ring breathing vibration; the calculated PED for this mode is 61%.

6.2. The CC Vibrations. The CC stretching vibrations of the title molecule occur in the region from 1000 to 1600 cm^{-1}. The majority of these modes of vibration are combined with CH and OH bending vibrations. The calculated PEDs for CC stretching are of about 13% for normal modes #37, #38, and #39. However the normal mode #40 is attributed to the CC stretching vibrations with a potential of 37% and less than 10% for normal modes #51 and #53. The CCC in-plane bending frequencies are found at 372, 443, 529, 618, 701, 860, and 923 cm^{-1}.

The CC torsions are likely to occur in the region below 500 cm^{-1}. For the title molecule, we found five normal modes representing the torsion about the bond $C_{12}C_{14}$. The calculated wavenumbers are 22, 79, 163, 265, and 325 cm^{-1}. The calculated PEDs are about 50%. These modes are not pure

Table 2: Frequencies and PEDs for 2-hydroxy-2-methyl-1-phenylpropan-1-one molecule.

[b]	Observed (cm^{-1})	DFT/6-311+G**			HF/6-311+G**	Assignment (%PED)[a]
		Unscaled (cm^{-1})	Scaled (cm^{-1})	Intensity ($km{\cdot}mol^{-1}$)	Scaled (cm^{-1})	
1	—	22.74	22.92	0.0053	17.23	$\tau(C_{12}C_{14})$ (68), $o(C_{12}C_{13})$ (22)
2	—	78.66	79.24	1.2078	72.16	$\tau(C_{12}C_{14})$ (48), $o(C_{14}O_{23})$ (26), $\tau(C_{14}C_{23})$ (15)
3	—	137.69	174.71	0.1931	133.22	$\tau(CH_3)$ (63), $o(C_{12}O_{13})$ (25)
4	—	162.19	163.17	0.1275	161.76	$\tau(C_{12}C_{14})$ (89)
5	—	184.98	186.03	0.0007	190.12	$\tau(CH_3)$ (76)
6	—	215.31	216.42	0.0829	218.35	$\tau(CH_3)$ (62), $\tau(C_{12}C_{14})$ (27)
7	—	257.12	258.28	0.2225	258.41	$\tau(CH_3)$ (63), $\rho(C_{14}O_{23})$ (14)
8	—	264.22	265.38	1.0193	261.87	$\tau(C_{12}C_{14})$ (54), $\delta(C_{12}C_{14}C_{19})$ (25), $\delta(C_{12}C_{14}C_{15})$ (14)
9	—	324.53	325.64	2.6572	318.84	$\tau(C_{12}C_{14})$ (54), $\delta(C_{12}C_{14}C_{19})$ (25)
10	—	371.29	372.27	4.4029	363.0228	$\delta(C_{12}C_{14}C_{15})$ (53), $\delta(C_{12}C_{14}C_{19})$ (26), $\delta(C_1C_{12}C_{14})$ (14),
11	—	415.70	416.5	12.5757	368.45	$o(O_{23}H)$ (51), $\tau(C_{14}O_{23})$ (25)
12	—	417.85	418.64	13.1148	418.74	$o(O_{23}H)$ (37), $\tau(C_{14}O_{23})$ (34), $o(O_{13}C_{12})$ (16)
13	—	442.58	443.24	23.2077	425.91	$\delta(C_{13}C_{12}C_{14})$ (79), $\delta(C_{12}C_{14}C_{15})$ (17)
14	—	444.60	445.25	39.0992	436.6872	$o(O_{23}H)$ (37), $o(C_1C_{12}O_{13})$ (28), $\rho(C_{12}C_{14}O_{23})$ (23)
15	—	506.39	506.62	13.7159	477.5168	$o(O_{23}H)$ (69), $\rho(C_{12}C_{14}O_{23})$ (20)
16	—	529.30	529.34	0.8797	524.676	$\delta(O_{13}C_{12}C_{14})$ (48), $\delta(C_1C_{12}C_{14})$ (45)
17	—	619.59	618.72	2.1280	611.3124	$\delta(C_{12}C_{14}C_{19})$ (44), $\delta(C_{12}C_{14}C_{15})$ (24), $\delta(O_{12}C_{13}C_{14})$ (15)
18	—	635.52	634.45	1.5297	623.346	Ring deformation (79), $\delta(C_1C_{12}C_{13})$ (17)
19	—	699.33	697.44	13.7753	689.55	$o(CH)_{ring}$ (62), $\delta(C_{12}C_{14}O_{23})$ (21)
20	—	703.85	701.89	11.8256	693.76	$\delta(C_1C_{12}C_{14})$ (68), $\delta(C_{12}C_{14}C_{15})$ (18)
21	716	723.68	721.43	72.3248	730.69	$o(C_{19}H_3)$ (53), $o(CH)_{ring}$ (23) $\tau(C_{12}C_{14})$ (17)
22	796	811.44	807.76	6.0346	815.01	$o(C_{15}H_3)$ (44), $\delta(O_{13}C_{12}C_{14})$ (24), $\delta(C_6C_1C_{12})$ (15), $o(O_{13}C_{12})$ (12)
23	836	862.56	857.93	0.2930	863.31	$o(CH)_{ring}$ (98)
24	856	865.50	860.82	1.4073	877.23	$\delta(C_{12}C_{14}C_{19})$ (67), $\delta(O_{13}C_{12}C_{14})$ (12)
25	—	929.00	923.01	0.0318	928.86	$\delta(C_{12}C_{14}O_{23})$ (41), $\delta(C_{12}C_{14}C_{15})$ (29), $\delta(C_{12}C_{14}C_{19})$ (13)
26	934	957.15	950.54	1.1541	958.57	$\delta(C_{12}C_{14}C_{15})$ (22), $\rho(C_{15}H_3)$ (19), $\rho(C_{15}H_3)$(17), $o(CH)_{ring}$ (14)
27	959	966.31	959.49	119.3931	978.08	$\nu(C_{14}O_{23})$ (83)
28	984	980.27	973.13	19.8320	997.34	$\rho(C_{19}H_3)$ (24), $\delta(C_1C_{12}C_{14})$ (24), $\nu(C_{14}O_{23})$ (22) $\rho(C_{14}O_{23}H)$ (12)
29	—	1002.21	994.55	0.2486	1000.37	$o(CH)_{ring}$ (53), $\rho(C_{15}H_3)$ (23), $\rho(C_{19}H_3)$ (21)
30	984	1016.36	1008.36	0.1061	1020.30	$\rho(C_{19}H_3)$ (68), $\rho(C_{15}H_3)$ (16)
31	—	1017.60	1009.57	3.5213	1026.49	Ring breathing (61), $\delta(C_{15}H_3)$ (21)
32	1004	1022.17	1014.03	0.4101	1031.95	$o(C_{19}H_3)$ (59), $\delta(C_{15}H_3)$ (28)
33	1034	1051.38	1042.50	2.1205	1034.20	$\rho(C_{15}H_3)$ (61), $\rho(19H_3)$ (18), $\beta(CH)_{ring}$ (15)
34	1077	1108.61	1098.22	4.6450	1082.28	$\beta(CH)_{ring}$ (72), $\beta(C_{15}H_3)$ (12)
35	1134	1163.52	1151.57	4.8064	1116.30	$\beta(C_{14}O_{23}H)$ (64), $\beta(C_{19}H_3)$ (26)
36	—	1182.42	1169.91	11.4215	1157.55	$o(C_{12}C_{14}O_{23})$ (48), $\rho(C_{15}H_3)$ (36), $\rho(C_{19}H_3)$ (14)
37	1170	1184.74	1172.16	164.1487	1186.76	$\beta(CH)_{ring}$ (40), $\delta(O_{23}H)$ (28), $\nu(C_1C_{12})$ (11)
38	—	1185.47	1172.87	43.3932	1193.31	$\rho(C_{15}H_3)$ (40), $\delta(O_{23}H)$ (21), $\nu(C_1C_{12})$ (13)
39	1192	1210.11	1196.76	10.7158	1210.98	$\beta(C_{15}H_3)$ (31), $\beta(CH)_{ring}$ (15), $\nu(C_{14}C_{19})$ (13)
40	1260	1263.08	1248.06	126.7838	1226.8	$\nu(C_1C_{12})$ (37), $\beta(C_{14}O_{23}H)$ (25), $\nu(C_{12}C_{14})$ (14)

Table 2: Continued.

[b]	Observed (cm^{-1})	DFT/6-311+G**			HF/6-311+G**	Assignment (%PED)[a]
		Unscaled (cm^{-1})	Scaled (cm^{-1})	Intensity ($km \cdot mol^{-1}$)	Scaled (cm^{-1})	
41	1280 sh	1332.76	1315.40	15.7006	1273.70	$\rho(C_{19}H_3)$ (49), $\rho(C_{15}H_3)$ (27)
42	1315	1350.99	1332.99	6.7816	1339.85	$\beta(CH)_{ring}$ (52), $\delta(C_{14}O_{23}H)$ (32),
43	1363	1385.14	1365.91	106.1420	1376.17	$\beta(C_{14}O_{23}H)$ (83)
44	1374	1397.17	1377.50	10.1008	1407.32	$\delta_{sym}(C_{19}H_3)$ (52), $\delta_{sym}(C_{15}H_3)$ (45)
45	1387	1418.22	1397.77	9.5326	1427.11	$\delta_{sym}(C_{19}H_3)$ (53), $\delta_{sym}(C_{15}H_3)$ (45)
46	—	1475.12	1452.48	0.6846	1463.36	$\rho(C_{19}H_3)$ (88), $\rho(C_{15}H_3)$ (8),
47	1447	1475.36	1452.71	7.9436	1466.61	$\nu(CC)_{ring}$ (65), $\delta(C_{15}H_3)$ (21)
48	—	1485.16	1462.12	1.4500	1477.58	$\delta_{asym}(C_{15}H_3)$ (47), $\delta_{asym}(C_{19}H_3)$ (41),
49	1457	1497.19	1473.67	14.4008	1487.97	$\delta_{asym}(C19H_3)$ (70)
50	1465	1504.27	1480.47	5.7803	1494.03	$\delta_{asym}(C_{19}H_3)$ (75), $\delta_{asym}(C_{15}H_3)$(17)
51	1489	1521.61	1497.10	0.3870	1517.46	$\nu(CC)_{ring}$ (51), $\delta(C_{15}H_3)$ (21)
52	1578	1615.70	1587.20	13.0932	1619.02	$\nu(CC)_{ring}$ (39), $\delta(C_{19}H_3)$ (37), $\delta(C_{15}H_3)$ (20)
53	1598	1636.91	1607.47	28.0759	1642.55	$\nu(CC)_{ring}$ (65), $\delta(CH)_{ring}$ (23)
54	1683	1710.11	1677.31	162.2382	1768.21	$\nu(C_{12}O_{13})$ (82)
55	2935	3042.17	2917.78	19.8324	2926.52	ν_{sym} CH of $(C_{19}H_3)$ (46), ν_{sym} CH of $(C_{15}H_3)$ (35)
56	—	3044.82	2920.19	8.9574	2931.07	ν_{sym} CH of $(C_{19}H_3)$ (50), ν_{sym} CH of $(C_{15}H_3)$ (29)
57	—	3107.42	2977.06	8.1447	2985.04	ν_{asym} CH of $(C_{19}H_{20}H_{21})$ (83)
58	2979	3109.66	2979.09	24.6775	2988.77	ν_{asym} CH of $(C_{19}H_{20}H_{21})$ (86)
59	2991	3124.55	2992.59	1.0567	3003.92	ν_{asym} CH of $(C_{19}H_3)$ (81)
60	—	3128.17	2995.88	48.0606	3012.34	ν_{asym} CH of $(C_{19}H_3)$ (83)
61	3025	3167.46	3031.48	0.2119	3058.37	$\nu(CH)_{ring}$ (93)
62	3060	3179.02	3041.94	10.4115	3071.30	$\nu(CH)_{ring}$ (94)
63	3070	3189.50	3051.43	14.3460	3082.53	$\nu(CH)_{ring}$ (95)
64	3090	3206.04	3066.38	5.7655	3109.14	$\nu(CH)_{ring}$ (89)
65	3108	3227.43	3085.72	5.2158	3131.98	$\nu(CH)_{ring}$ (85)
66	3458	3670.40	3482.74	117.92	3781.02	$\nu(OH)$ (85)

[a] Assignments and potential energy distribution (PED) (contributing > 10%) for vibrational normal mode. Types of vibration: ν: stretching; δ: deformation; o: out-of-plane bending; β: in-plane bending; ρ: rocking; τ: torsion; sym: symmetric; asym: asymmetric.
[b] Normal mode number.

thereby they are generally mixed with other CO and CH_3 torsions.

6.3. The C=O Vibrations. The C=O stretch of carboxylic acids is identical to the C=O stretch in ketones, which is expected in the region 1740–1660 cm^{-1} [28]. Krishnakumar et al. [29] observed very strong band at 1661 cm^{-1} in the IR spectrum for 1-naphthyl acetic acid, and it is assigned to the C=O stretching vibrations. In the present work a strong band observed in the FTIR spectrum at 1683 cm^{-1} is assigned to the C=O stretching vibrations. The calculated peak is at 1677 cm^{-1} with PED value of 82% as reported in Table 2.

6.4. The COH Vibrations. The CO stretching vibration is assigned to the band at 959 cm^{-1} in the FTIR spectrum. The predicted frequency shows a good correlation. The PED value is 83% for mode #27 and 22% for mode #28; most of the CO vibrations are mixed vibrations as shown in Table 2.

The OH group gives rise to three vibrations, namely, stretching, in-plane bending, and out-of-plane bending. The OH group vibrations are likely to be the most sensitive to the environment, so they show pronounced shifts in the spectra of the hydrogen-bonded species. In the case of unsubstituted phenol it has been shown that the frequency of OH stretching vibration in the gas phase is 3657 cm^{-1} [27]. Subramanian et al. [30] report the infrared spectrum of 2,5-di-tert-butylhydroquinone and assign the strong band at 3402 cm^{-1} to the OH stretching vibration. Koczon et al. [22] studied the experimental and theoretical IR and Raman spectra of picolinic, nicotinic, and isonicotinic acids and assigned the bands at 3437, 3447, and 3436 cm^{-1} for these molecules to the OH stretching vibration. In the FTIR spectrum of the title compound, the band observed at 3458 cm^{-1} is assigned to the OH stretching mode. The computed wavenumber is at 3482 cm^{-1} with a PED value of 85%. The carboxylic acids show in-plane bending band of OH at 1134 cm^{-1} (FTIR). This band is well reproduced

by the calculated and scaled one at 1151 cm^{-1}. The PED calculation predicts the existence of another OH in-plane bending at 1365 cm^{-1}. This band is well correlated with the one at 1363 cm^{-1} in the experimental infrared spectrum. The calculated frequencies at 416, 418, 445, 506, and 807 cm^{-1} are assigned to the OH out-of-plane bending. The last band is well correlated with the experimental one at 796 cm^{-1}. These normal modes are mixed with the skeleton bending vibrations and torsions. The predicted PEDs are about 50%.

6.5. The Methyl Group Vibrations. For the assignment of CH_3 group frequencies, nine fundamentals can be associated to each CH_3 group [31–33]. The CH stretching in CH_3 occurs at lower frequencies than those of aromatic ring (3100, 3000 cm^{-1}). Moreover, the asymmetric stretch is usually at higher wavenumber than the symmetric stretch. In the present work, in the experimental spectrum the CH_3 asymmetric stretching frequency is assigned to the bands at 2991 and 2979 cm^{-1}, whereas the symmetric stretching frequency is assigned to the band at 2935 cm^{-1}. These bands are well reproduced by the calculated ones at 2995, 2992, 2979, and 2977 cm^{-1} for the asymmetric stretching and 2920, 2917 cm^{-1} for the symmetric stretching vibrations. The PED values for these normal modes are greater than 70%.

For methyl substituted benzene derivatives, the antisymmetric and symmetric deformation vibrations of methyl group normally appear in the region 1465–1440 cm^{-1} and 1390–1370 cm^{-1}, respectively [21, 31, 34]. We attributed the observed doublet in the FTIR spectrum at 1465 and 1457 cm^{-1} to the asymmetric deformation of CH_3 vibrations. These bands are well correlated with those calculated at 1480, 1473, and 1462 cm^{-1} with PED values greater than 80%. The bands at 1374 and 1387 cm^{-1} (FTIR) are assigned to the symmetric CH_3 deformation. The simulated frequencies at 1397 and 1377 cm^{-1} represent good correlations for the symmetric CH_3 deformations. The normal modes no. 28, #30, #33, #38, and #41 are assigned to the CH_3 rocking vibrations. These vibrations find location with the CH ring bending vibrations in the range from 984 to 1280 cm^{-1}. This is in concordance with Subramanian et al. [30] assignments of the infrared bands of 2, 5-di-tert-butyl-hydroquinone. They reported that the rocking vibrations of methyl group for this molecule take location in the range from 837 to 1247 cm^{-1}, and they are mixed with the CH ring vibrations.

7. HOMO-LUMO Analysis

The total energy, energy gap, and dipole moment have an effect on the stability of a molecule. In this work we calculate these parameters for title compound in gas phase and solvent. For this purpose we used B3LYP/6-311+G** level of theory. Obtained results are reported in Table 3.

The energy gap between the HOMO and LUMO is an important parameter in determining molecular electrical transport proprieties and molecular stability. The energy gap between the HOMO and the LUMO is a critical parameter in determining the molecular electrical transport proprieties because it is a measure of electron conductivity. The energy values of HOMO are computed −7.456, −7.374, and −7.401 eV and LUMO are −2.231, −2.204, and −2.258 eV, and the energy gap values are 5.225, 5.17, and 5.143 eV in gas phase, DMSO and chlorophorm for 2-hydroxy-2-methyl-1-phenylpropan-1-one molecule, respectively. Lower value of the energy gap explains the eventual charge transfer interactions taking place within the molecule. In order to understand the bonding scheme of the title molecule we draw the surfaces of the orbitals frontier. We examine the four important molecular orbitals: the highest and the second highest occupied MOs and the lowest and the second lowest unoccupied MOs. These molecular orbitals are represented in Figure 6.

Table 3: Calculated energies of 2-hydroxy-2-methyl-1-phenylpropan-1-one in gas, DMSO, and chloroform.

DFT/B3LYP/6-311+G**	Gas	DMSO	Chloroform
E_{total} (hartree)	−538.8921	−538.9054	−538.9013
E_{HOMO} (eV)	−7.456	−7.374	−7.401
E_{LUMO} (eV)	−2.231	−2.204	−2.258
$\Delta E_{HOMO-LUMO\ gap}$ (eV)	5.225	5.17	5.143
E_{HOMO-1} (eV)	−7.592	−7.483	−7.510
E_{LUMO+1} (eV)	−0.925	−0.707	−0.734
$\Delta E_{HOMO-1-LUMO+1\ gap}$ (eV)	6.667	6.776	6.776
Dipole moment (Debye)	4.1536	5.6353	5.1924

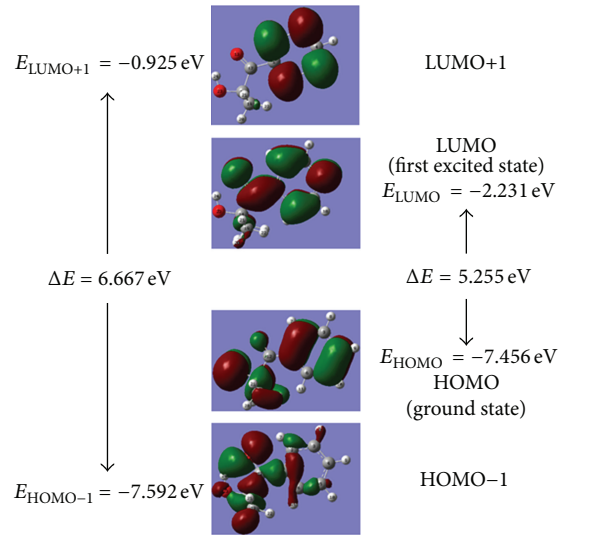

Figure 6: Molecular orbital frontier of 2-hydroxy-2-methyl-1-phenylpropan-1-one: representation of the HOMO, HOMO-1, LUMO, and LUMO+1 orbitals.

According to Figure 6 the charge distribution for the HOMO is localized on the C=C ring, OH, and CH of methyl group. The LUMO is characterized by a charge distribution at CH bond on the ring and C_1C_{12} bond.

8. Conclusions

A meticulous conformational search of the title molecule leads to a unique stable conformation. For this purpose

the calculations were conducted with reliable DFT and HF levels of theory using 6-311+G** basis set. The fully optimized geometries at HF and DFT (B3LYP) were compared with the experimental data of related compounds presented in the literature. The comparison shows a good agreement. Infrared spectra were recorded, and the vibrational bands were assigned on the basis of the PED calculations obtained from B3LYP/6-311+G** calculations. A very good agreement between the observed and the calculated wavenumbers was observed. The scaled frequencies at HF/6-311+G** level of theory are in general greater than those calculated at B3LYP/6-311+G**. The latter ones are more accurate. Through the molecular orbital analysis we found that the energy gap between HOMO and LUMO is lower; this would explain the eventual charge transfer in the title molecule.

References

[1] N. S. Allen, "Photoinitiators for UV and visible curing of coatings: mechanisms and properties," *Journal of Photochemistry and Photobiology A*, vol. 100, no. 1–3, pp. 101–107, 1996.

[2] J. P. Fouassier, *Photoinitiation, Photopolymerization and Photocuring*, Hanser Publishers, Munich, Germany, 1995.

[3] B. Seidl, R. Liska, and G. Grabner, "New photocleavable structures III: photochemistry and photophysics of pyridinoyl and benzoyl-based photoinitiators," *Journal of Photochemistry and Photobiology A*, vol. 180, no. 1-2, pp. 109–117, 2006.

[4] H. Kaczmarek and I. Vukovic-Kwiatkowska, "Preparation and characterization of interpenetrating networks based on polyacrylates and poly(lactic acid)," *eXPRESS Polymer Letters*, vol. 6, no. 1, pp. 78–94, 2012.

[5] G. A. Sim, J. M. Robertson, and T. H. Goodwin, "The crystal and molecular structure of benzoic acid," *Acta Crystallographica*, vol. 8, pp. 157–164, 1955.

[6] F. J. Strieter and D. H. Templeton, "Crystal structure of butyric acid," *Acta Crystallographica*, vol. 15, pp. 1240–1244, 1962.

[7] P. S. Binil, Y. S. Mary, H. T. Varghese, C. Yohannan Panicker, M. R. Anoop, and T. K. Manujkumar, "Infrared and Raman spectroscopic analyses and theoretical computation of 4-butyl-1-(4-hydroxyphenyl)-2-phenyl-3,5-pyrazolidinedione," *Spectrochimica Acta Part A*, vol. 94, pp. 101–109, 2012.

[8] L. Lecamp, B. Youssef, C. Bunel, and P. Lebaudy, "Photoinitiated polymerization of a dimethacrylate oligomer—part 2: kinetic studies," *Polymer*, vol. 40, no. 6, pp. 1403–1409, 1999.

[9] F. Burel, L. Lecamp, B. Youssef, C. Bunel, and J. M. Saiter, "Synthesis and photoinitiated polymerization of a new urethane acrylate monomer: influence of polymerization temperature," *Thermochimica Acta*, vol. 326, no. 1-2, pp. 133–141, 1999.

[10] L. Lecamp, B. Youssef, C. Bunel, and P. Lebaudy, "Photoinitiatedpolymerization of a dimethacrylate oligomer—part 3: postpolymerization study," *Polymer*, vol. 40, no. 23, pp. 6313–6320, 1999.

[11] H. Xu, F. Qiu, Y. Wang, W. Wu, D. Yang, and Q. Guo, "UV-curable waterborne polyurethane-acrylate: preparation, characterization and properties," *Progress in Organic Coatings*, vol. 73, no. 1, pp. 47–53, 2012.

[12] L. Lecamp, B. Youssef, C. Bunel, and P. Lebaudy, "Photoinitiated polymerization of a dimethacrylate oligomer: 1. Influence of photoinitiator concentration, temperature and light intensity," *Polymer*, vol. 38, no. 25, pp. 6089–6096, 1997.

[13] A. D. Becke, "Density-functional thermochemistry. III. The role of exact exchange," *The Journal of Chemical Physics*, vol. 98, no. 7, pp. 5648–5652, 1993.

[14] C. Lee, W. Yang, and R. G. Parr, "Development of the Colle-Salvetti correlation-energy formula into a functional of the electron density," *Physical Review B*, vol. 37, no. 2, pp. 785–789, 1988.

[15] V. K. Rastogi, M. A. Palafox, R. P. Tanwar, and L. Mittal, "3,5-difluorobenzonitrile: Ab initio calculations, FTIR and Raman spectra," *Spectrochimica Acta Part A*, vol. 58, no. 9, pp. 1987–2004, 2002.

[16] H. Yoshida, A. Ehara, and H. Matssura, "Density functional vibrational analysis using wavenumber-linear scale factors," *Chemical Physics Letters*, vol. 325, no. 4, pp. 477–483, 2000.

[17] J. Baker, A. A. Jarzecki, and P. Pulay, "Direct scaling of primitive valence force constants: an alternative approach to scaled quantum mechanical force fields," *Journal of Physical Chemistry A*, vol. 102, no. 8, pp. 1412–1424, 1998.

[18] M. J. Frisch, G. W. Trucks, H. B. Schlegel et al., *Gaussian 03, Revision B.01*, Gaussian, Inc., Pittsburgh, Pa, USA, 2003.

[19] J. M. L. Martin and C. van Alsenoy, *GAR2PED: A Program to obtain a Potential Energy Distribution from a Gaussian Archive Record*, University of Antwerp, Antwerp, Belgium, 2009.

[20] P. Pulay, G. Fogarasi, F. Pang, and J. E. Boggs, "Systematic ab initio gradient calculation of molecular geometries, force constants, and dipole moment derivatives," *Journal of the American Chemical Society*, vol. 101, no. 10, pp. 2550–2560, 1979.

[21] M. Silverstein, G. C. Basseler, and C. Morill, *Spectrometric Identification of Organic Compounds*, Wiley, New York, NY, USA, 1981.

[22] P. Koczon, J. Cz. Dobrowolski, W. Lewandowski, and A. P. Mazurek, "Experimental and theoretical IR and Raman spectra of picolinic, nicotinic and isonicotinic acids," *Journal of Molecular Structure*, vol. 655, no. 1, pp. 89–95, 2003.

[23] M. Karabacak, Z. Cinar, M. Kurt, S. Sudha, and N. Sundaraganesan, "FT-IR, FT-Raman, NMR and UV-vis spectra, vibrational assignments and DFT calculations of 4-butyl benzoic acid," *Spectrochimica Acta Part A*, vol. 85, no. 1, pp. 179–189, 2012.

[24] P. B. Nagabalasubramanian, M. Karabacak, and S. Periandy, "FT-IR, FT-Raman, ab initio and DFT structural, vibrational frequency and HOMO-LUMO analysis of 1-naphthaleneacetic acid methyl ester," *Spectrochimica Acta Part A*, vol. 82, no. 1, pp. 169–180, 2011.

[25] N. B. Colthup, L. H. Daly, and S. E. Wiberley, *Introduction to Infrared and Raman Spectroscopy*, Academic Press, New York, NY, USA, 1964.

[26] L. J. Bellamy, *The Infrared Spectra of Complex Molecules*, Chapman and Hall, 1980.

[27] G. Varsanyi, *Assignments for Vibrational Spectra of Seven Hundred Benzene Derivatives*, vol. 1-2, Adam Hilger, 1974.

[28] D. L. Vein, N. B. Colthup, W. G. Fateley, and J. G. Grasselli, *The Handbook of Infrared and Raman Characteristic Frequencies of Organic Molecules*, Academic Press, San Diego, Calif, USA, 1991.

[29] V. Krishnakumar, R. Mathammal, and S. Muthunatesan, "FT-IR and Raman spectra vibrational assignments and density functional calculations of 1-naphthyl acetic acid," *Spectrochimica Acta Part A*, vol. 70, no. 1, pp. 210–216, 2008.

[30] N. Subramanian, N. Sundaraganesan, O. Dereli, and E. Turkkan, "FT-IR, FT-Raman spectra, density functional computations of the vibrational spectra and molecular conformational analysis of 2,5-di-tert-butyl-hydroquinone," *Spectrochimica Acta Part A*, vol. 83, no. 1, pp. 165–174, 2011.

[31] E. B. Wilson, J. C. Decius, and P. C. Cross, *Molecular Vibrations: The Theory of Infrared and Raman Vibrational Spectra*, McGraw-Hill Book Company, New York, NY, USA, 1955.

[32] O. Dereli, Y. Erdogdu, M. T. Gulluogu, E. Turkkan, A. Ozmen, and N. Sundaraganesan, "Vibrational spectral and quantum chemical investigations of tert-butyl-hydroquinone," *Journal of Molecular Structure*, vol. 1012, pp. 168–176, 2012.

[33] P. Chinna Babu, N. Sundaraganesan, O. Dereli, and E. Türkkan, "FT-IR, FT-Raman spectra, density functional computations of the vibrational spectra and molecular geometry of butylated hydroxy toluene," *Spectrochimica Acta Part A*, vol. 79, no. 3, pp. 562–569, 2011.

[34] S. Kalaichelvan, N. Sundaraganesan, O. Dereli, and U. Saying, "Experimental, theoretical calculations of the vibrational spectra and conformational analysis of 2,4-di-tert-butylphenol," *Spectrochimica Acta Part A*, vol. 85, no. 1, pp. 198–209, 2012.